Petrology, Vol. 8, No. 2, 2000, pp. 145–160. Translated from Petrologiya, Vol. 8, No. 2, 2000, pp. 165–181.

Reaction Textures and Metamorphic Evolution of Spinel Granulites in the Voronezh Crystalline Massif

K. A. Savko

Voronezh State University, Universitetskaya pl. 1, Voronezh, 394693 Russia
e-mail: gfkig304@main.vsu.ru

Received March 20, 1999

Abstract—The Early Archean high-Al granulites in the Central megablock of the Voronezh crystalline massif bear three types of mineral assemblages: (I) *Qtz–Spl*$_{Zn\geqslant}$*–Crd–Sil–Bt–Py–Mag*, (II) *Qtz–Grt–Crd–Sil–Spl*$_{Zn>}$*–Bt–Mag–Ilm*, and (III) *Qtz–Kfs–Grt–Crd–Sil–Spl–Mag–Ilm–Py*. Diverse reaction textures typical of mineral assemblages of type I include pyrite rims around spinel (separating it from quartz and sillimanite) and thin cordierite rinds around spinel (separating it from quartz). The reaction textures of assemblage (II) are spinel–quartz inclusions in garnet, cordierite rims surrounding spinel grains, magnetite inclusions in sillimanite, and sillimanite rims around magnetite–ilmenite and spinel–magnetite aggregates. The metapelites with assemblage (III) were determined to bear double plagioclase–cordierite rims around spinel and cordierite–sillimanite rims around sulfide aggregates. The pyrite rims around spinel and cordierite–sillimanite rims around sulfides were produced by cordierite and spinel sulfidization as a consequence of a sulfur activity increase late during the metamorphic evolution. The *P–T* trajectory of the retrograde stage demonstrates the subisobaric cooling of the granulites from 800–810°C and 7.6–7.8 kbar to 595°C and 5 kbar. The metamorphic evolution of the spinel granulites was caused by the extension of the crust, which had been thickened during the Early Proterozoic collision, and the reduction of its thickness to its normal level.

INTRODUCTION

Aluminous granulites with spinel commonly contain diverse mineral assemblages sensitive to *P–T* metamorphic conditions. The rocks usually abound in diverse corona textures, which can be used as indicators of successive prograde and retrograde metamorphic reactions. Hence, spinel granulites may provide valuable information on the evolution of the *P–T* metamorphic conditions and can be used in reconstructing the geodynamic environments of high-temperature metamorphism. Although numerous reaction textures in spinel granulites can help in interpreting metamorphic events, it is necessary to analyze these mineral equilibria taking into account additional factors, such as the presence of Zn, Ti, and Fe^{3+} in the system.

Spinel–quartz granulites with cordierite, sillimanite, and garnet bear mineral assemblages indicative of high-temperature metamorphism under mid-crustal conditions, at temperatures above 800°C and pressures in the range of 4–7 kbar. Spinel granulites typically display *P–T* paths of isobaric cooling after the metamorphic culmination (Clarke *et al.*, 1989; Perchuk *et al.*, 1989; Sengupta *et al.*, 1991; Warren and Stewart, 1988; Waters, 1991; and others), although decompression-controlled *P–T* trajectories of these rocks were also described (Clarke and Powell, 1991).

The spinel granulites examined in the central portion of the Voronezh crystalline massif contain diverse corona textures. The spinel of these textures varies in composition and coexists with sulfides in some coronas or with oxides in others, a fact testifying to very wide variations in the oxygen and sulfur fugacities.

This paper is devoted to mineral assemblages and reaction textures in spinel granulites from the Voronezh crystalline massif, their *P–T* paths, and tectonic interpretations of the metamorphic events.

GEOLOGY

The two Archean blocks currently recognized in the Voronezh crystalline massif, Central (Kursk–Besedino) and Bryansk, are made up of compositionally variable rocks metamorphosed to the granulite facies. The Central block is dominated by eulysites, metabasites, metaultrabasites, and metapelites, whereas the Bryansk block contains widespread granulites of intermediate composition ("metadiorites"), metapelites, eulysites, and marbles.

The Central block is a second-order structure, which is situated in the central part of the Kursk Magnetic Anomaly megablock, more precisely, in the central part of the Kursk anticlinorium, which is composed mainly of Early Archean supracrustal rocks of the Oboyan Group. The anticlinorium is an uplift of the Precambrian basement of the Voronezh crystalline massif, which separates the Mikhailovsko–Belgorod and Orel–Timskii greenstone belts. The Kursk–Besedino megablock is made up of biotite and biotite–hornblende plagiogneisses with thin beds of hornblende amphibolites, which are often migmatized and gran-

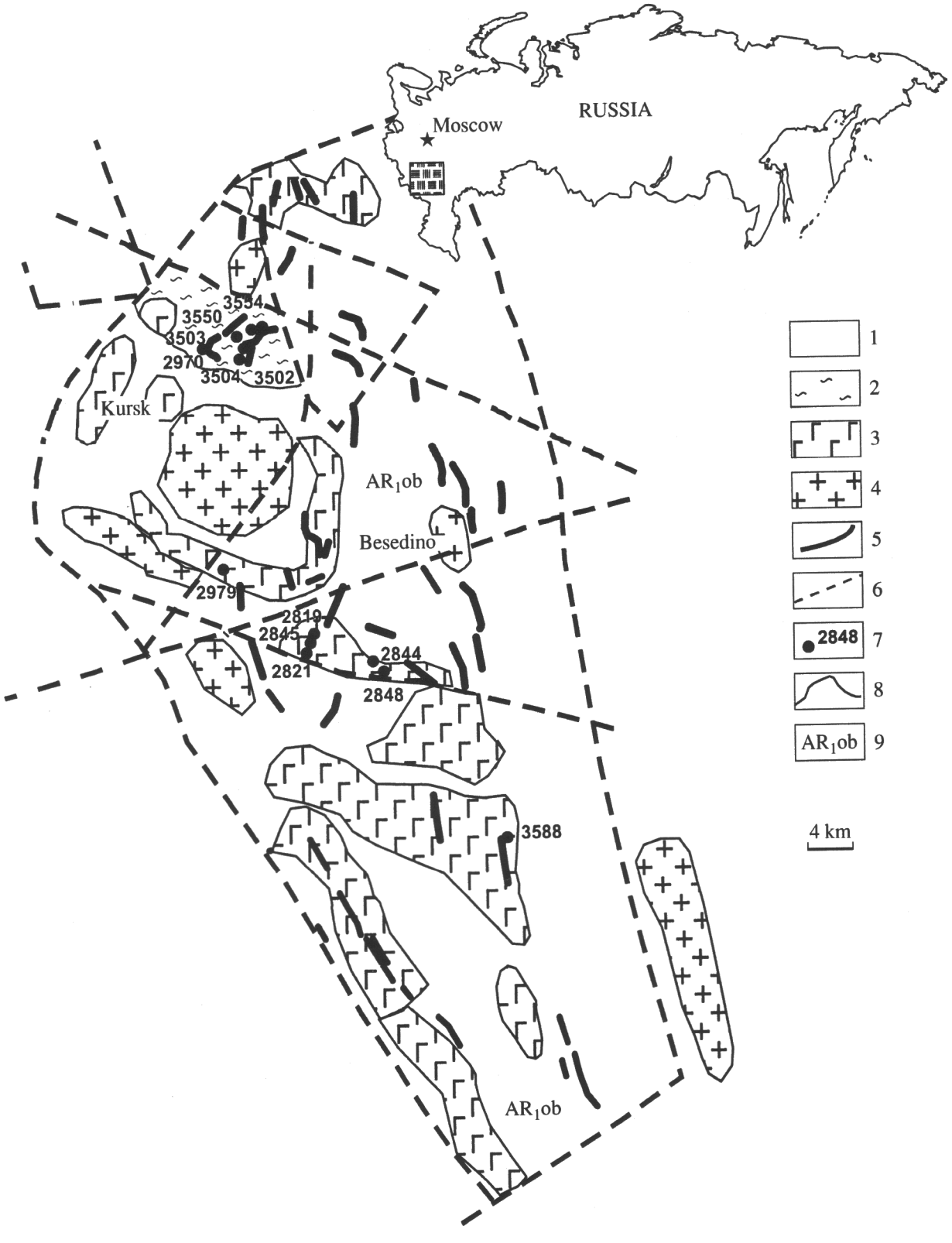

Fig. 1. Schematic geological map of the central block of the Voronezh crystalline massif.
(1) Undifferentiated plagiogneisses and migmatites of the Oboyan Group; (2) aluminous metapelites; (3) metagabbroids and metapyroxenites; (4) microcline and plagioclase–microcline granites; (5) eulysites; (6) faults; (7) drill holes and their numbers; (8) geologic boundaries; (9) index of the Oboyan Group. The shaded square in the map of Russia shows the location of the Voronezh crystalline massif.

itized. The gneiss complex is characterized by an overall mosaic pattern of its magnetic field with intense positive anomalies (Ushakovskie, Kuvshinovskie, Budanovskie, Besedino, etc.) of ellipsoidal, crescent, or stripe-like morphology, which correspond to compositionally variable rocks metamorphosed to the granulite facies. Drilling materials indicate that the rock succession is composed of relatively thin (from 1–2 to 30–35 m) strata of eulysites, metapyroxenites, metagabbroids, and metapelites. Granulites with spinel-bearing assemblages were reliably detected only in the Ushakovskie anomalies and were penetrated by Holes 3504, 3550, and 3554 (Fig. 1).

Unfortunately, currently there is only one relatively reliable determination of the age of rocks from the Kursk–Besedino block. The $^{207}Pb/^{206}Pb$ zircon age of the granite-gneiss recovered by Hole 3588 is 3178 ± 3 Ma (Artemenko, 1995). No isochron was constructed because of the closeness of the U–Pb ratios.

PETROGRAPHY

The metapelitic granulites are pale gray and gray massive or unclearly banded medium- or coarse-grained gneisses. The textures of the rocks are granoblastic, lepido-granoblastic, and porphyroblastic. The porphyroblasts are garnet crystals up to 1 cm in diameter. The mineral assemblages can be subdivided into three types: (I) $Qtz + Spl_{Zn\gg} + Crd + Sil + Bt + Py \pm Mag$ (Sample 3550/9), (II) $Qtz + Grt + Crd + Sil + Spl_{Zn>} + Bt + Mag$ (Sample 3550/6), and $Qtz + Crd + Sil + Spl_{Zn>} + Bt + Mag + Ilm$ (Sample 3504/183, and (III) $Qtz + Kfs + Grt + Crd + Sil + Spl + Mag + Ilm + Py$ (Samples 3554/143a and 3554/143b). In the assemblages of type I, spinel accounts for 5–20 modal % and very often occurs in physical contact with quartz. The reaction textures typical of mineral assemblages of type (I) include pyrite rims around spinel (which separate it from quartz and sillimanite, with the pyrite sometimes replaced by magnetite; Figs. 2a, 2b, 3a) and thin cordierite selvages around spinel (which separate it from quartz, with the cordierite sometimes replaced by secondary chlorite; Figs. 2a, 2b). The reaction textures of assemblage (II) are spinel and quartz inclusions in garnet, with spinel often occurring in contact with magnetite (Figs. 4a, 5a, 5b), cordierite rims around spinel and garnet (Fig. 4b), magnetite inclusions in sillimanite (Fig. 4b), and sillimanite rims around magnetite–spinel and magnetite–ilmenite aggregates (Figs. 6a, 6b). In the metapelites with mineral assemblage (III), some spinel grains are armored by cordierite and complex rims with inner cordierite and outer plagioclase parts (Fig. 3b). These rims separate the spinel from quartz and potassic feldspar. Another type of reaction textures is cordierite–sillimanite rims surrounding sulfide aggregates, which consist of pyrite, pyrrhotite, and chalcopyrite (Figs. 7a, 7b). The spinel contains magnetite exsolution textures (Fig. 3b).

METHODS

All samples of the granulites are fragments of the core of holes, which was thoroughly described during the fieldwork. The selected samples were examined optically, and minerals from rocks in which metamorphic reaction textures were detected were studied on a laser microprobe. The analyses of minerals were conducted on a Camebax SX-50 (at the Moscow State University) at an accelerating potential of 15 kV, beam current of 1–2 nA, and a beam size of 1–2 μm. The accuracy of analyses was systematically controlled with the use of natural and synthetic standard reference samples. The cation proportions of minerals were normalized to 12 oxygens for garnet, 4 oxygens for spinel, 18 oxygens for cordierite, 11 oxygens for biotite, 5 oxygens for sillimanite, and 8 oxygens for potassic feldspar. The reflected-electron images of reaction textures were obtained on a CamScan electron microscope (at the Moscow State University). The *P–T* metamorphic conditions and a_{H_2O} were calculated by the TPF (Fonarev *et al.*, 1991) and GEOPATH (Gerya and Perchuk, 1992) computer packages.

MINERAL CHEMISTRY

The composition of *spinel* varies depending on the mineral assemblage. In garnet-free assemblage (I), the spinel is very high in Zn (from 16.8 to 21.4 wt %), i.e., corresponds to gahnite with admixtures of the hercynite, spinel, and magnetite end-members (Table 1). Because of the high Zn concentration of the spinel, its Fe mole fraction is relatively low, 0.481–0.513 at 20.0–21.4 wt % ZnO and 0.555–0.606 at 16.8–17.7 wt % ZnO, with the Fe mole fraction slightly increasing from the cores to margins of most grains. The distribution of Zn is unsystematic, except that the maximum concentrations pervasively occur at contacts of some spinel grains with quartz. The spinel of assemblage (I) is characterized by relatively high contents of Fe_2O_3, which attain a maximum in the most zincian varieties. The Fe_2O_3 concentrations, calculated based on stoichiometric considerations, vary from 2.73 to 3.59 wt % at 20.0–21.4 wt % ZnO and from 0.93 to 1.85 wt % at 16.8–17.7 wt % ZnO.

In Sample 3550/6 (with assemblages of type II), the spinel is more ferrous (X_{Fe} = 0.678–0.747) and higher in Zn (7.6–10.9 wt % ZnO; Table 1). The most ferrous (X_{Fe} = 0.74) and the least zincian spinel was detected in inclusions in garnet, and the highest Zn concentrations (10.88 wt % ZnO) were detected in spinel surrounded by cordierite in the rock matrix. The Fe_2O_3 concentrations in spinel from this type of assemblages are relatively low and do not exceed 0.47 wt %, except a spinel inclusion in garnet with 0.94 wt % ZnO. The spinel detected in the garnet-free rock of Sample 3504/183 is surrounded by a sillimanite rim and is low in Zn (7.41–7.61 wt % ZnO) and more ferrous (X_{Fe} = 0.78).

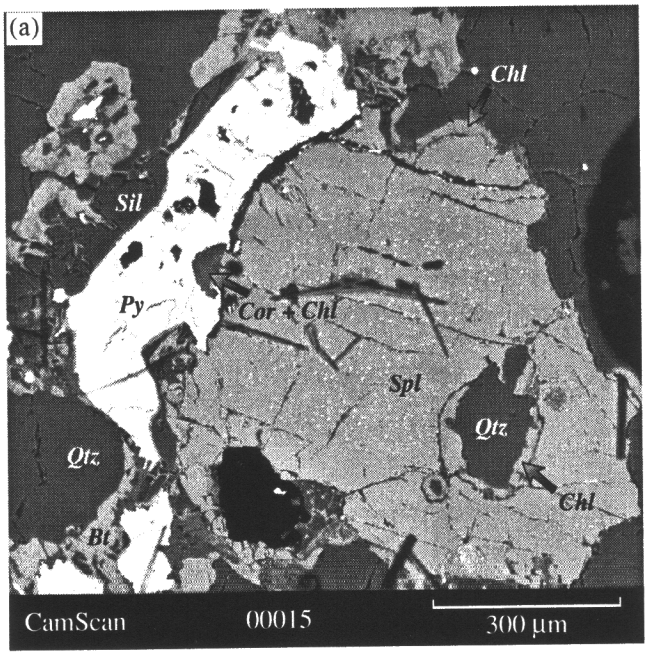

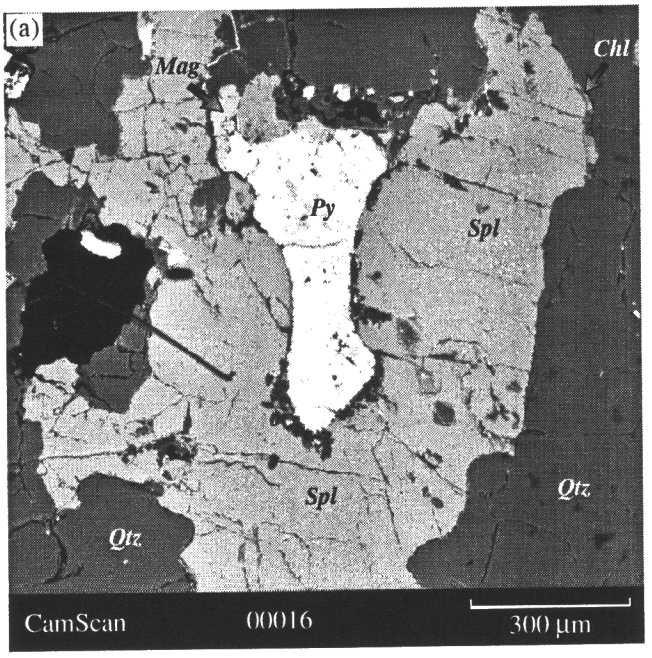

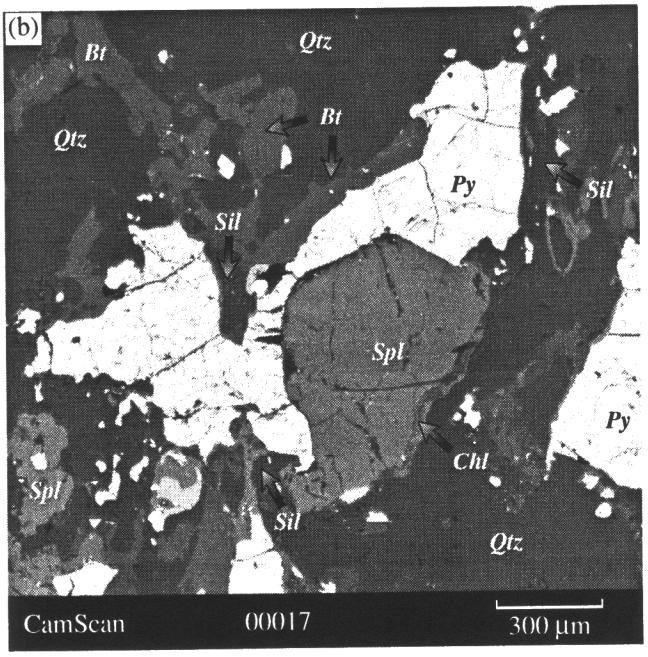

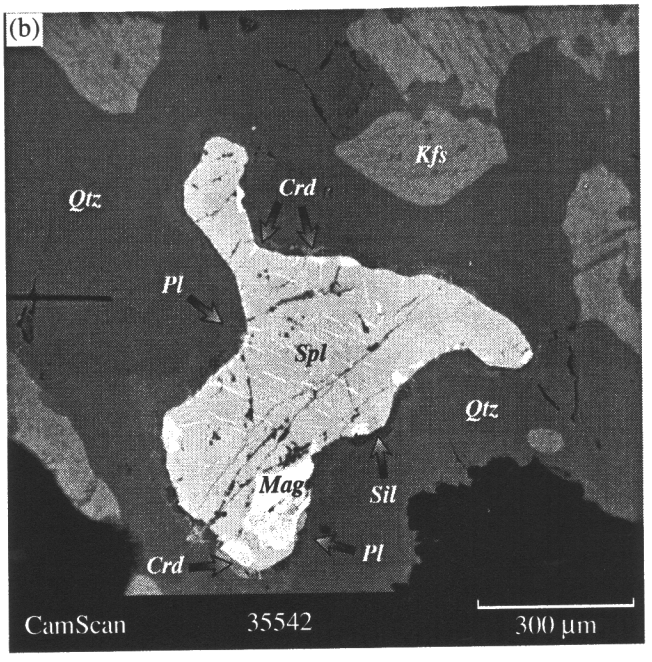

Fig. 2. Back-scattered electron image of reaction textures in spinel granulites from the Kursk–Besedino block.
(a) Pyrite and chlorite rims around spinel. Secondary chlorite replaces cordierite.
(b) Sillimanite–pyrite rims around spinel. Sample 3550/9.
Images were obtained on a CamScan electron microscope.

Fig. 3. Back-scattered electron image of reaction textures in spinel granulites from the Kursk–Besedino block.
(a) Quartz and Zn-rich spinel in physical contact. Sample 3550/9.
(b) Plagioclase–cordierite rim around spinel; thin magnetite lamellae in the spinel are exsolution textures. Sample 3554/143a.
Images were obtained on a CamScan electron microscope.

The spinel in mineral assemblage (III) has X_{Fe} = 0.728–0.767 and is low in Zn (0.81–2.38 wt % ZnO) and fairly high in Cr (3.4–4.6 wt % Cr_2O_3; Table 1). The V_2O_3 concentrations of the spinel never exceed 0.45 wt %. No compositional zoning was detected in individual spinel crystals. Fairly high Fe_2O_3 concentrations (up to 4–5 wt %) are obtained when the analyses were recalculated in compliance with the stoichiometry of the mineral. This is most probably caused by the presence of magnetite exsolution lamellae (Fig. 3b), as was pre-

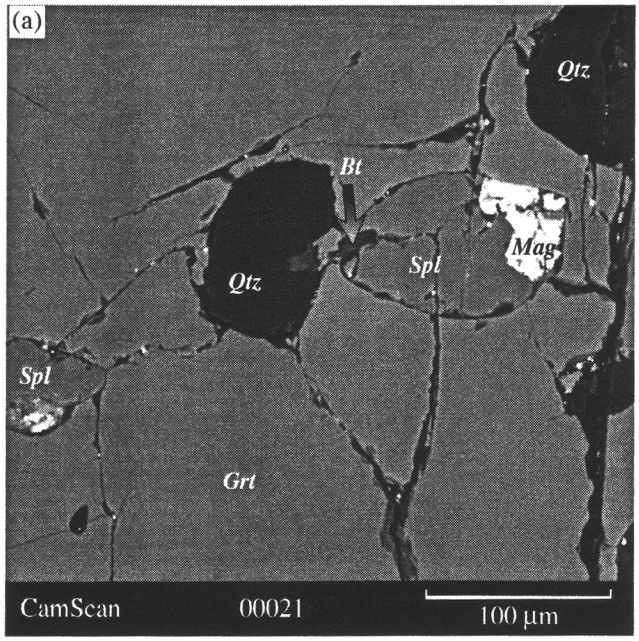

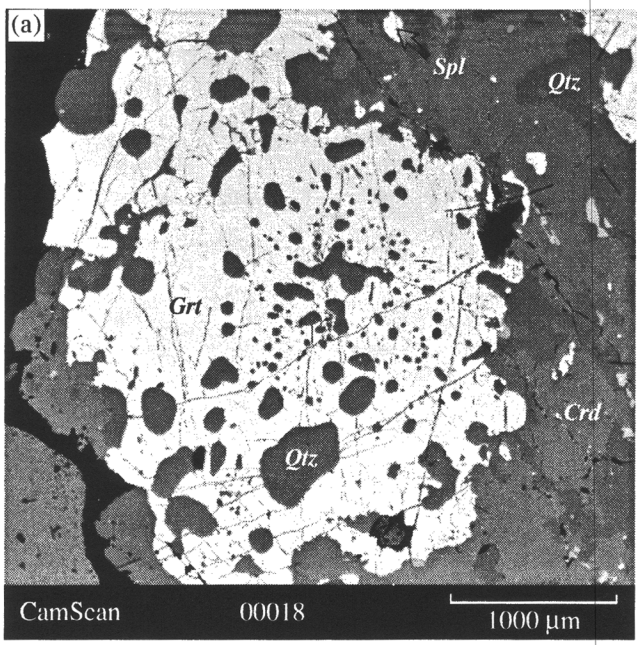

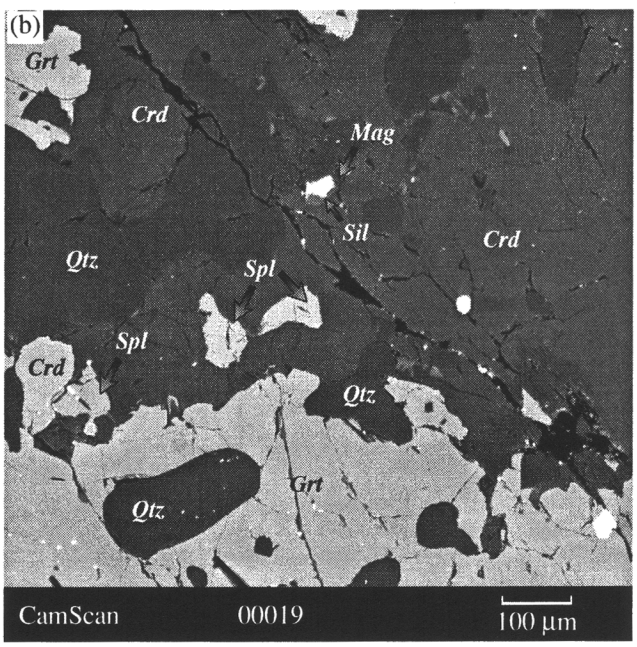

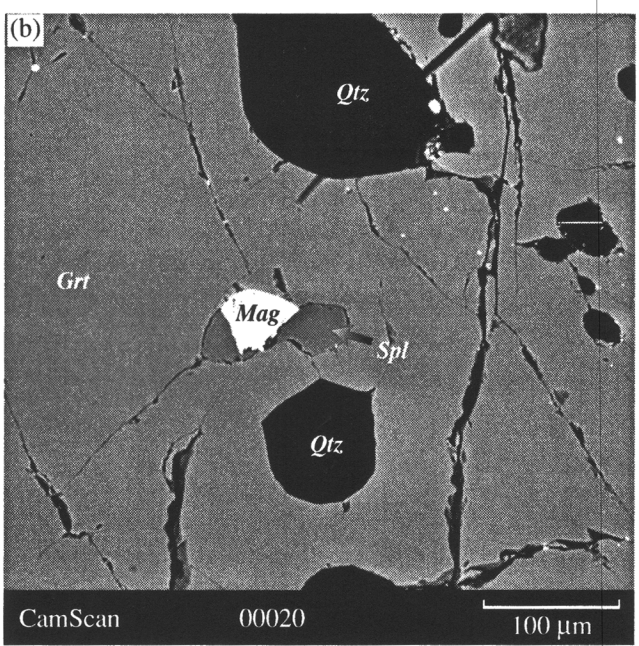

Fig. 4. Back-scattered electron image of reaction textures in spinel granulites from the Kursk–Besedino block.
(a) Quartz, spinel, and magnetite inclusions in garnet.
(b) Cordierite rims around spinel and sillimanite–magnetite aggregates. Sample 3550/6.
Images were obtained on a CamScan electron microscope.

Fig. 5. Back-scattered electron image of reaction textures in spinel granulites from the Kursk–Besedino block.
(a) Large garnet grain with numerous quartz and spinel inclusions.
(b) Quartz, spinel, and magnetite inclusions in garnet. Sample 3550/6.
Images were obtained on a CamScan electron microscope.

viously described by many researchers (Waters, 1991; Dasgupta *et al.*, 1995; and others).

Garnet is present in assemblages (II) and (III), in which it commonly occurs as large crystals, often with resorbed outlines and numerous inclusions of quartz, biotite, spinel, and sillimanite. The garnet displays no compositional zoning, excluding thin outermost zones at contacts with biotite and cordierite, where X_{Fe} increases and X_{Mg} decreases. In the garnet in Sample 3550/6, X_{Mg} is 0.350–0.362 in the core and 0.326 at contacts with cordierite. A similar tendency was observed in Samples 3554/143a and 3554/143b: in the

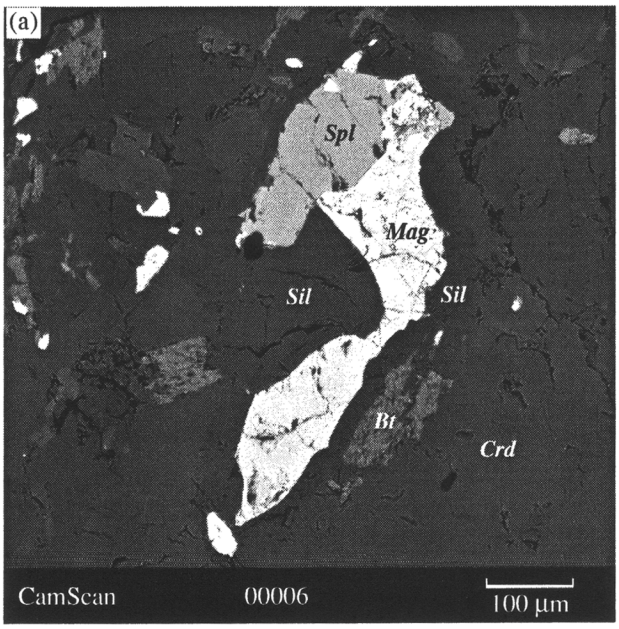

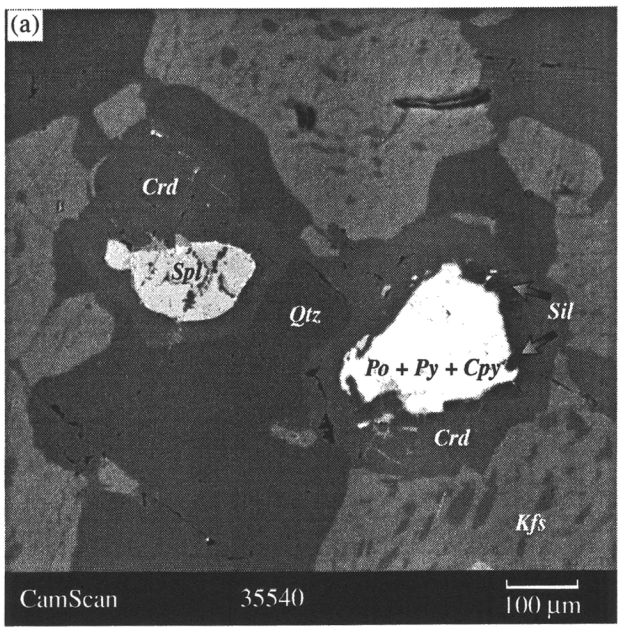

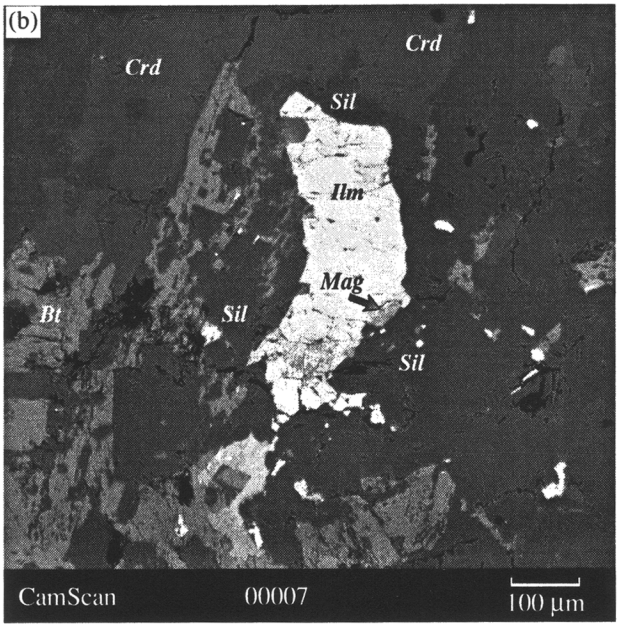

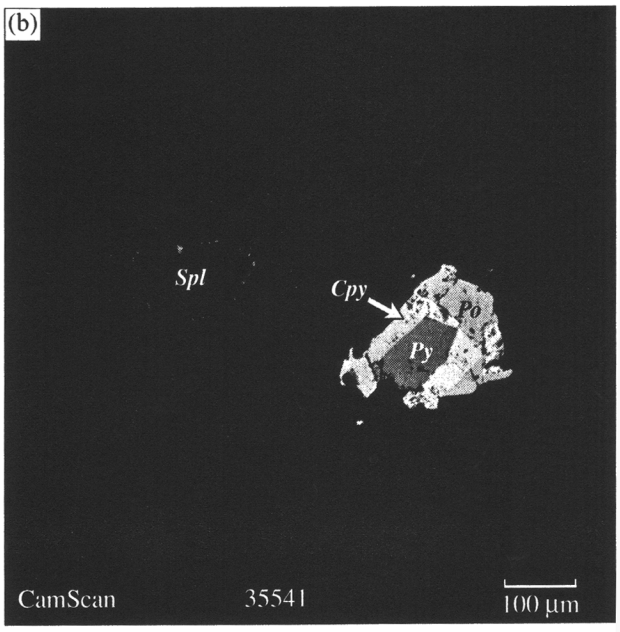

Fig. 6. Back-scattered electron image of reaction textures in spinel granulites from the Kursk–Besedino block.
(a) Sillimanite rim around a magnetite–spinel aggregate.
(b) Sillimanite rim around an ilmenite grain with magnetite exsolution lamellae. Sample 3504/183.
Images were obtained on a CamScan electron microscope.

Fig. 7. Back-scattered electron image of reaction textures in spinel granulites from the Kursk–Besedino block.
(a) Cordierite rim around spinel and a cordierite–sillimanite rims around a sulfide aggregate.
(b) Internal structure of a sulfide aggregate: pyrite is rimmed by chalcopyrite and pyrrhotite. Sample 3554/143a.
Images were obtained on a CamScan electron microscope.

former, X_{Mg} decreases from 0.325–0.336 in the core to 0.269 at contacts with cordierite, and in the latter, this parameter varies from 0.393–0.394 in the core to 0.342 at contacts with biotite (Table 2). The CaO and MnO concentrations are low, usually no more than 1 wt % and show no systematic zonal distribution.

Cordierite that forms reaction rims around spinel ir assemblage (I) is fully replaced by chlorite; thus, its composition was not analyzed. The cordierite of mineral assemblage (II) is characterized by X_{Mg} from 0.787 to 0.813, with this parameter increasing at contacts with garnet. In assemblage (III), the cordierite is less

Table 1. Composition (wt %) of spinel and magnetite from metapelitic granulites in the central part of the Voronezh crystalline massif

Component	3550/9									3550/6				3554/143b
	grain with a *Py + Sil rim*			in *Qtz* matrix			in *Qtz* matrix with a *Py* rim			inclusion in *Grt*		in matrix		in matrix
	margin	core	margin	margin	core	margin	core	margin	margin with a *Qtz* inclusion	in *Grt* core	in *Grt* margin	core	core	core
	Py		*Qtz*	*Py*		*Qtz*		*Py*				*Grt*		*Crd*
	Spl-3	*Spl*-4	*Spl*-5	*Spl*-12	*Spl*-13	*Spl*-14	*Spl*-18	*Spl*-19	*Spl*-24	*Spl*-6	*Spl*-7	*Spl*-8	*Spl*-9	*Spl*-77
SiO_2	–	–	–	–	–	–	–	–	–	–	–	–	–	0.05
TiO_2	–	–	–	–	–	–	–	–	–	–	–	–	–	0.07
Al_2O_3	55.03	55.56	56.41	58.05	58.55	57.49	57.61	57.58	57.02	59.33	60.34	60.21	59.52	58.21
Cr_2O_3	0.57	0.46	–	0.40	–	0.63	0.46	0.49	0.64	–	–	–	–	0.67
FeO	17.20	16.04	15.90	18.66	17.65	17.53	17.49	17.31	18.98	27.44	24.96	25.58	24.85	29.43
MnO	–	–	–	–	–	–	–	0.48	–	0.47	–	–	–	0.07
MgO	6.57	6.87	6.26	5.86	5.87	5.93	6.66	6.13	5.99	5.14	6.44	6.06	4.63	6.97
ZnO	20.05	20.52	21.40	16.83	17.51	17.66	17.61	18.00	16.92	7.66	8.16	7.99	10.88	3.60
Total	99.42	99.45	99.97	99.80	99.58	99.24	99.83	99.99	99.55	100.04	99.90	99.84	99.88	99.07
Si	–	–	–	–	–	–	–	–	–	–	–	–	–	0.001
Ti	–	–	–	–	–	–	–	–	–	–	–	–	–	0.001
Al	1.866	1.877	1.901	1.946	1.963	1.940	1.925	1.929	1.920	1.968	1.983	1.984	1.988	1.924
Cr	0.013	0.010	–	0.009	–	0.014	0.010	0.011	0.014	–	–	–	–	0.015
Fe^{3+}	0.121	0.112	0.099	0.045	0.037	0.046	0.065	0.060	0.066	0.032	0.017	0.016	0.012	0.055
Fe^{2+}	0.292	0.272	0.281	0.398	0.383	0.374	0.350	0.351	0.388	0.614	0.564	0.582	0.577	0.635
Mn	–	–	–	–	–	–	–	0.012	–	0.011	–	–	–	0.002
Mg	0.282	0.294	0.267	0.248	0.249	0.253	0.281	0.260	0.255	0.216	0.268	0.253	0.196	0.291
Zn	0.426	0.434	0.452	0.353	0.368	0.373	0.369	0.378	0.357	0.159	0.168	0.165	0.228	0.075
X_{Fe}	0.509	0.481	0.513	0.617	0.606	0.603	0.555	0.574	0.603	0.740	0.678	0.697	0.747	0.686

Component	3554/143a									3504/183				
	grain with a *Crd* rim		grain with a *Crd + Pl rim*		*Spl–Mag* inclusion	*Crd* matrix	inclusion in *Spl*	small grain	in contact with *Grt*	*Spl–Mag* aggregate with a *Sil* rim			*Mag–Ilm* aggregate	
	core	margin	core	margin			core	margin		margin	core	core	core	core
		Mag		*Crd*	*Sil*			*Spl*		*Sil*		*Spl*	*Ilm*	*Sil*
	Spl-2	*Spl*-3	*Spl*-5	*Spl*-6	*Spl*-8	*Spl*-10	*Mag*-7	*Mag*-9	*Ilm*-15	*Spl*-5	*Spl*-4	*Mag*-6	*Mag*-7	*Ilm*-8
SiO_2	0.02	0.20	–	0.02	0.31	0.03	0.01	–	0.35	–	–	0.32	0.24	–
TiO_2	0.03	0.02	0.03	0.04	0.03	0.04	0.02	0.05	48.21	0.01	0.02	0.04	0.06	46.16
Al_2O_3	52.64	52.57	52.87	52.63	51.80	52.55	0.16	0.20	–	52.30	51.29	0.82	0.81	0.02
Cr_2O_3	3.63	3.47	3.40	3.43	4.56	3.46	2.28	3.11	–	3.70	3.49	3.69	5.09	0.35
FeO	36.96	36.86	35.65	36.03	35.35	35.82	97.40	96.53	49.69	32.08	32.64	94.62	93.19	53.08
MnO	0.10	0.12	0.22	0.13	0.12	0.13	0.06	0.05	–	0.02	0.11	–	0.02	0.10
MgO	5.60	5.68	6.23	6.25	5.47	5.17	–	0.01	0.69	4.22	4.26	0.26	0.19	0.10
ZnO	1.01	0.99	0.81	0.85	2.38	2.19	–	–	–	7.61	7.41	–	–	–
Total	99.99	99.91	99.21	99.38	100.02	99.39	99.93	99.95	98.94	99.94	99.22	99.75	99.60	99.81
Si	0.001	0.006	–	0.001	0.009	0.001	–	–	0.009	–	–	0.011	0.009	–
Ti	0.001	–	0.001	0.001	0.001	0.001	0.001	0.001	0.916	–	–	0.001	0.002	0.872
Al	1.772	1.770	1.782	1.773	1.752	1.785	0.007	0.008	–	1.790	1.770	0.035	0.034	0.001
Cr	0.082	0.078	0.077	0.077	0.103	0.079	0.065	0.088	–	0.085	0.081	0.105	0.145	0.007
Fe^{3+}	0.144	0.140	0.140	0.147	0.126	0.133	1.927	1.901	0.151	0.125	0.148	1.836	1.801	0.249
Fe^{2+}	0.739	0.741	0.713	0.714	0.722	0.730	0.999	0.999	0.899	0.654	0.652	0.999	0.999	0.866
Mn	0.002	0.003	0.005	0.003	0.003	0.003	0.002	0.002	–	–	0.003	–	0.001	0.002
Mg	0.238	0.242	0.266	0.266	0.234	0.222	–	0.001	0.026	0.183	0.186	0.014	0.010	0.004
Zn	0.021	0.021	0.017	0.018	0.050	0.047	–	–	–	0.163	0.160	–	–	–
X_{Fe}	0.756	0.754	0.728	0.728	0.755	0.767	–	–	–	0.781	0.778	–	–	0.998

Note: Fe^{3+} was calculated based on stoichiometric considerations; $X_{Fe} = Fe^{2+}/(Fe^{2+} + Mg)$.

Table 2. Composition (wt %) of garnet from spinel granulites in the central part of the Voronezh crystalline massif

Component	3550/6					3554/143a							
	large grain with *Spl*, *Qtz*, and *Mag* inclusions					large *Grt* with sillimanite inclusions in the matrix							
	core	margin	margin	margin	core	margin	→	→	→	core		margin	margin
			Spl	*Crd*		*Crd*						*Ilm*	*Qtz*
	Grt-1	*Grt*-2	*Grt*-3	*Grt*-4	*Grt*-5	*Grt*-1	*Grt*-2	*Grt*-3	*Grt*-4	*Grt*-6	*Grt*-8	*Grt*-12	*Grt*-14
SiO_2	39.99	39.83	39.47	40.27	40.30	39.60	39.56	39.62	39.55	39.75	38.92	38.54	39.18
Al_2O_3	21.52	22.16	21.77	21.80	22.03	21.38	21.67	21.65	21.56	21.71	21.75	22.04	22.14
FeO	28.74	28.17	28.76	28.97	27.87	31.32	29.72	29.19	29.56	29.00	29.42	31.13	29.35
MnO	0.89	0.81	0.63	0.97	0.64	0.70	0.63	0.58	0.62	0.50	0.60	0.66	0.52
MgO	8.33	8.64	8.68	7.85	8.89	6.45	7.74	8.24	7.99	8.14	8.34	6.96	8.25
CaO	0.65	0.52	0.69	0.39	0.47	0.71	0.77	0.77	0.76	0.99	0.87	0.61	0.57
Total	100.12	100.13	100.00	100.25	100.20	100.16	100.09	100.05	100.04	100.09	99.90	99.94	100.01
Alm	0.634	0.625	0.629	0.652	0.620	0.705	0.658	0.642	0.651	0.640	0.639	0.692	0.648
Sps	0.020	0.018	0.014	0.022	0.014	0.016	0.014	0.013	0.014	0.012	0.013	0.015	0.012
Prp	0.328	0.342	0.338	0.315	0.352	0.259	0.306	0.323	0.314	0.320	0.323	0.276	0.325
Grs	0.018	0.015	0.019	0.011	0.013	0.020	0.022	0.022	0.021	0.028	0.024	0.017	0.016
X_{Mg}	0.340	0.353	0.350	0.326	0.362	0.269	0.327	0.335	0.325	0.333	0.336	0.285	0.334

Component	3554/143a					3554/143b				
	large grain with sillimanite inclusions					large grain with biotite inclusions				
	core				margin	margin	core	margin	core	margin
					Crd	*Bt*		*Crd*		*Bt*
	Grt-5	*Grt*-7	*Grt*-9	*Grt*-11	*Grt*-13	*Grt*-65	*Grt*-66	*Grt*-70	*Grt*-72	*Grt*-76
SiO_2	39.62	39.92	39.62	39.69	38.84	38.86	38.71	38.56	38.70	38.62
Al_2O_3	21.66	21.68	21.80	21.88	21.36	22.06	21.87	21.71	21.92	22.05
FeO	29.92	28.85	29.30	28.94	30.50	28.57	27.34	28.88	27.49	28.93
MnO	0.48	0.64	0.72	0.65	0.71	0.54	0.52	0.70	0.39	0.51
MgO	7.82	8.07	8.01	8.00	7.72	8.78	10.09	8.93	10.16	8.59
CaO	0.60	0.98	0.64	0.94	0.77	0.96	0.83	0.78	0.95	1.12
Total	100.10	100.14	100.09	100.10	99.90	99.77	99.36	99.56	99.61	99.82
Alm	0.663	0.639	0.649	0.642	0.664	0.621	0.563	0.621	0.582	0.626
Sps	0.011	0.014	0.016	0.015	0.016	0.012	0.011	0.015	0.008	0.011
Prp	0.309	0.319	0.316	0.316	0.299	0.340	0.383	0.342	0.384	0.331
Grs	0.017	0.028	0.018	0.027	0.021	0.027	0.023	0.021	0.026	0.032
X_{Mg}	0.318	0.333	0.328	0.330	0.311	0.350	0.393	0.350	0.394	0.342

Note: $X_{Mg} = Mg/(Fe^{2+} + Mg)$.

magnesian (X_{Mg} = 0.772–0.803). The most ferrous cordierite (X_{Mg} = 0.733) was encountered in the rock matrix, and the most magnesian (X_{Mg} = 0.780–0.803) one occurs at contacts with garnet. The grains occurring in contact with garnet are zoned, with X_{Mg} increasing from the core to margin (Table 3). Intermediate X_{Mg} values (0.751–0.761) were detected in cordierite rims around spinel.

Sillimanite is present in all mineral assemblages and participates in reaction textures. In mineral assemblage (I), sillimanite and pyrite compose rims around spinel (Figs. 2a, 2b). In assemblage (II), sillimanite occurs in a cordierite matrix and develops as rims around spinel–magnetite and ilmenite–magnetite aggregates (Figs. 6a, 6b). The sillimanite of assemblage (III) occurs as inclusions in garnet or in rims around sulfides (Fig. 7a). The

Table 3. Composition (wt %) of cordierite from spinel granulites in the central part of the Voronezh crystalline massif

Component	3554/143a									
	grain in contact with *Grt*			grain in contact with *Grt*			matrix	rim around *Spl*		
	matrix	core	core	matrix	core	matrix	core			
	Grt					*Grt*	*Bt*	*Spl, Pl*	*Spl*	
	Crd-21	*Crd*-22	*Crd*-23	*Crd*-24	*Crd*-25	*Crd*-26	*Crd*-27	*Crd*-3	*Crd*-6	*Crd*-7
SiO_2	52.21	52.31	52.47	52.12	52.99	53.68	52.69	46.25	45.96	45.32
Al_2O_3	33.82	33.74	33.56	33.45	33.04	33.77	33.26	31.89	32.53	32.98
FeO	4.39	4.96	4.83	4.63	4.85	4.41	5.75	7.66	8.06	7.99
MgO	10.01	9.48	9.62	10.15	9.67	8.97	8.87	13.66	13.66	13.78
CaO	–	–	–	–	–	–	–	0.09	–	–
Total	100.43	100.49	100.48	100.35	100.55	100.83	100.57	99.55	100.21	100.07
Si	5.141	5.158	5.171	5.144	5.216	5.248	5.205	4.734	4.681	4.624
Al	3.925	3.921	3.898	3.981	3.833	3.891	3.872	3.847	3.904	3.965
Fe	0.361	0.409	0.398	0.382	0.399	0.361	0.475	0.656	0.686	0.682
Mg	1.469	1.393	1.413	1.493	1.419	1.307	1.306	2.084	2.074	2.096
Ca	–	–	–	–	–	–	–	0.010	–	–
X_{Mg}	0.803	0.773	0.780	0.796	0.780	0.784	0.733	0.761	0.751	0.755

Component	3550/6			3504/183			3554/143b
	large grains in matrix			grains in matrix			
	core	margin	margin	core	margin	margin	core
	Grt		*Spl*		*Sil*	*Sil*	*Grt*
	Crd-10	*Crd*-11	*Crd*-12	*Crd*-30	*Crd*-32	*Crd*-34	*Crd*-69
SiO_2	51.92	51.19	51.17	50.36	50.14	50.08	50.46
Al_2O_3	34.07	34.63	34.62	32.29	32.36	32.27	33.95
FeO	4.61	4.43	4.21	5.58	5.74	6.00	3.33
MgO	9.58	10.02	10.26	11.53	11.48	11.37	11.22
CaO	0.23	–	–	–	–	–	0.08
Na_2O				0.09	0.17	0.07	
Total	100.41	100.27	100.26	99.85	99.89	99.79	99.07
Si	5.122	5.056	5.051	5.043	5.026	5.029	5.031
Al	3.961	4.031	4.027	3.811	3.823	3.819	3.989
Fe	0.380	0.366	0.347	0.467	0.481	0.504	0.278
Mg	1.409	1.475	1.510	1.721	1.715	1.702	1.668
Ca	0.024	–	–	–	–	–	0.009
Na				0.017	0.033	0.014	
X_{Mg}	0.787	0.801	0.813	0.786	0.781	0.772	0.857

mineral contains an admixture of Fe_2O_3 (up to 1.29 wt %, Table 4).

Biotite is present in most of the samples in low amounts (no more than 5 modal %). The biotite in the matrix has the lowest X_{Mg} (0.560–0.665), a red–brown color, and a moderate TiO_2 concentration (4.03–4.29 wt %; Table 4). The biotite crystallizing at contacts with garnet is more magnesian (X_{Mg} = 0.806–0.812) and less titanic. The biotite included in garnet has X_{Mg} = 0.654 and contains 3.30 wt % TiO_2. The most magnesian biotite (X_{Mg} = 0.881) was detected in the garnet-free rock of Sample 3550/9.

Table 4. Composition (wt %) of biotite, potassic feldspar, and sillimanite from metapelitic granulites in the central part of the Voronezh crystalline massif

Component	3554/143a				3554/143b						3550/9			3504/183	
	matrix		matrix		inclusion in *Grt*	matrix					matrix	in rims with *Py*		rim around *Spl, Mag, Ilm*	
	margin	core	core	margin		margin	margin	core	margin		margin				
	Grt	*Grt*		*Crd*	*Grt*	*Crd*		*Grt*	*Crd*	*Spl*				*Spl*	*Ilm*
	Bt-16	*Bt*-28	*Kfs*-17	*Kfs*-18	*Bt*-67	*Bt*-68	*Bt*-73	*Bt*-74	*Bt*-75	*Sil*-4	*Bt*-8	*Sil*-9	*Sil*-20	*Sil*-31	*Sil*-33
SiO_2	38.55	38.02	65.34	65.37	36.06	38.63	37.24	36.64	39.03	33.97	39.13	37.42	36.18	38.11	37.35
TiO_2	3.24	4.29	–	–	3.30	4.03	2.97	4.11	0.71	–	3.11	–	–	–	–
Al_2O_3	17.28	16.83	17.81	17.86	15.49	15.74	16.69	16.15	17.21	64.88	15.60	61.69	62.70	60.56	61.12
Cr_2O_3	0.46	–	–	–	0.24	0.21	0.18	0.30	0.27	–	–	–	–		–
FeO	12.81	16.39	–	–	15.92	8.19	13.24	13.55	8.50	1.29	11.50	0.87	1.01	1.00	0.69
MnO	–	–	–	–	–	–	–	0.07	–	–	–	–	–	–	–
MgO	14.42	11.71	–	–	16.88	19.11	16.91	15.19	20.59	–	17.51	–			–
CaO	0.31	0.25	–	0.24	0.10	0.02	0.04	–	0.08	–	–	–	–		–
Na_2O	–	–	0.97	1.07	–	0.10	–	0.22	–	–	–	–	–	0.07	0.05
K_2O	10.00	9.79	15.81	15.43	7.01	9.48	8.22	9.28	9.01	0.02	9.57	–	–	0.01	0.01
Total	97.07	97.28	99.93	99.97	95.00	95.51	95.49	95.51	95.40	100.16	96.42	99.98	99.89	99.75	99.22
Si	2.790	2.790	3.018	3.015	2.684	2.779	2.727	2.713	2.797	0.928	2.826	1.013	0.983	1.035	1.018
Ti	0.176	0.237	–	–	0.185	0.218	0.164	0.229	0.038	–	0.169	–	–	–	–
Al(IV)	1.210	1.210	0.970	0.971	1.316	1.221	1.273	1.287	1.223	2.076	1.174	1.969	2.008	1.937	1.964
Al(VI)	0.264	0.245	–	–	0.042	0.114	0.167	0.123	0.250	–	0.153	–	–		–
Cr	0.026	–	–	–	0.014	0.012	0.010	0.018	0.015	–	–	–	–		–
Fe	0.775	1.006	–	–	0.991	0.493	0.811	0.839	0.509	0.029	0.694	0.020	0.023	0.023	0.016
Mn	–	–	–	–	–	–	–	0.004	–	–	–	–	–	–	–
Mg	1.556	1.281	–	–	1.873	2.020	1.846	1.677	2.184	–	1.885	–	–	–	–
Ca	0.024	0.020	–	0.012	0.008	–	–	–	0.006		–	–	–	–	–
Na	–	–	0.087	0.096	–	0.014	–	0.032	–	–	–	–	–	0.004	0.003
K	0.923	0.916	0.932	0.908	0.666	0.857	0.768	0.877	0.824	0.001	0.881	–	–	–	–
X_{Mg}	0.667	0.560			0.654	0.806	0.695	0.665	0.812		0.731				

Magnetite is a common mineral of the rocks, in which it occurs in the reaction textures described above and in the form of thin exsolution lamellae in spinel. Compositionally, the mineral is nearly pure magnetite with minor admixtures of Al_2O_3 and Cr_2O_3. The magnetite in aggregates with spinel and ilmenite contains from 3.5 to 5 wt % Cr_2O_3 and 0.8 wt % Al_2O_3 (Table 1).

Ilmenite occurs more rarely than magnetite and mainly in the rock matrix. In assemblage (II), ilmenite–magnetite aggregates are rimmed by sillimanite (Fig. 6b).

Sulfides are mainly pyrite, which forms reaction rims around spinel in assemblage (I) and also occurs in cordierite-armored aggregates with pyrrhotite and chalcopyrite in assemblage (III). The composition of the mineral corresponds to practically pure pyrite without admixtures of other components, including Zn.

INTERPRETATION OF REACTION TEXTURES AND MINERAL EQUILIBRIA

The aforementioned reaction textures provide evidence of mineral reactions that proceeded in the metapelites after the metamorphic culmination; i.e., they reflect the retrograde metamorphic stage. The very high concentrations of the gahnite end-member in the spinel of assemblage (I) suggest that the rock contained a Zn-rich staurolite. Phase relations during the breakdown of Zn-rich staurolite with the formation of spinel, sillimanite, and cordierite (or garnet) were described by many authors in papers dealing with zonal contact-metamorphic complexes (Guidotti, 1974; Korikovsky, 1979; Savko, 1997).

The presence of oxides (magnetite and ilmenite) in the reaction textures with spinel is quite common and was documented in many granulite complexes (Per-

chuk *et al.*, 1989; Dasgupta *et al.*, 1995; and others). Pyrite rims in association with sillimanite replacing spinel are much more rare, and their development during the retrograde metamorphic stage was possible only at a high sulfur activity. Pyrite in assemblage with sillimanite could be formed by the sulfidization of spinel in accordance with the reaction

$$\underset{(Spl)}{FeAl_2O_4} + \underset{(Otz)}{SiO_2} + S_2 \longrightarrow \underset{(Py)}{FeS_2} + \underset{(Sil)}{Al_2SiO_5} + 3O_2 \quad (1)$$

or by the sulfidization of cordierite in rims around spinel in accordance with the reaction

$$\underset{(Crd)}{Fe_2Al_4Si_5O_{18}} + 2S_2 \longrightarrow \underset{(Py)}{2FeS_2} + \underset{(Sil)}{2Al_2SiO_5} + \underset{(Otz)}{3SiO_2} + O_2. \quad (2)$$

The cordierite rims around spinel were produced by the reaction

$$Spl + Qtz \longrightarrow Crd. \quad (3)$$

In mineral assemblage (II), spinel and quartz inclusions in garnet indicate that these minerals coexisted during the metamorphic culmination, after which the reaction

$$Spl + Qtz \longrightarrow Grt + Sil \quad (4)$$

took place. The cordierite rims around spinel were produced by reaction (3), and the rims around garnet (Fig. 4b), by reaction

$$Grt + Qtz + Sil \longrightarrow Crd. \quad (5)$$

The sillimanite rims around spinel–magnetite aggregates (Fig. 6a) may have been formed during spinel oxidation

$$\underset{(Spl)}{3FeAl_2O_4} + \underset{(Qtz)}{3SiO_2} + 0.5O_2 \longrightarrow \underset{(Sil)}{3Al_2SiO_5} + \underset{(Mag)}{Fe_3O_4} \quad (6)$$

or

$$\underset{(Spl)}{9FeAl_2O_4} + \underset{(Crd)}{3Fe_2Al_4Si_5O_{18}} + 5O_2 \longrightarrow \underset{(Sil)}{15Al_2SiO_5} + \underset{(Mag)}{5Fe_3O_4}. \quad (7)$$

The crystallization of magnetite during the decomposition of spinel is corroborated by the elevated Cr_2O_3 and Al_2O_3 concentrations of the former mineral (Table 1). Aggregates of magnetite and ilmenite can be interpreted as the exsolution products of ulvospinel solid solution (Sengupta *et al.*, 1991; Waters, 1991)

$$6Fe_2TiO_4 + O_2 \longrightarrow 6FeTiO_3 + 2Fe_3O_4. \quad (8)$$

This reaction is shifted to the right with decreasing temperature.

In assemblage (III), cordierite rims that separate spinel from quartz were produced by reaction (3), and the plagioclase rims (Fig. 3b) resulted from reaction

$$Spl + Qtz + Na^+ + Ca^{2+} \longrightarrow Pl + Fe^{2+} + Mg^{2+}. \quad (9)$$

The appearance of aggregates of sillimanite, pyrite, and cordierite (Figs. 6a, 6b) was caused by the sulfidization of spinel and cordierite at an increasing sulfur activity, for example,

$$\underset{(Spl)}{3FeAl_2O_4} + \underset{(Crd)}{Fe_2Al_4Si_5O_{18}} + 5S_2 \longrightarrow \underset{(Py)}{5FeS_2} + \underset{(Sil)}{5Al_2SiO_5} + 2.5O_2. \quad (10)$$

METAMORPHIC *P–T* CONDITIONS

In order to draw the *P–T* metamorphic path of the metapelitic granulites from the Voronezh crystalline massif, it was necessary to estimate the *P–T* conditions during the metamorphic culmination and the retrograde stage after it (based on the information "recorded" in the reaction textures described above). The *P–T* conditions of metapelitic granulites can be assayed by the garnet–cordierite–sillimanite–quartz geothermobarometer (Aranovich and Podlesskii, 1989; Perchuk *et al.*, 1984), spinel–cordierite–quartz geobarometer (Perchuk *et al.*, 1989), and the spinel–cordierite geothermometer (Vielzeuf, 1983; Perchuk *et al.*, 1989; Gerya and Perchuk, 1990).

The peak temperatures and pressures were evaluated by the compositions of the cores of large magnesian garnet crystals and the most ferrous cordierite in the rock matrix. The rest of our estimates were obtained for the marginal portions of garnet grains and cordierite in contact with garnet or for cordierite rims around spinel and pertain to the retrograde *P–T* evolution of the rocks.

The most realistic results seem to be the *P–T* parameters evaluated by the set of consistent thermometers and barometers (Aranovich and Podlesskii, 1989; Perchuk *et al.*, 1984) and independent procedures for the calculation of the temperature and pressure (Table 5). The temperatures calculated by these thermobarometers were correlated with the analogous values calculated by other garnet–cordierite thermometers at a given pressure for each mineral assemblage (Table 5). All values coincide within 5–7°C, a fact testifying to the reliability of the estimates. The maximum values (804°C and 7.7 kbar), which are close to the conditions during the metamorphic culmination, were yielded by a core of a large garnet crystal and matrix cordierite from Sample 3554a. The minimum values (595°C and 5.0 kbar) were calculated for garnet margins and adjacent cordierite from Sample 3554/143a. Intermediate values define a linear trend between the two extremal points (Fig. 8, trend I).

Table 5. *P–T* conditions of mineral equilibria estimated by the garnet–cordierite and garnet–cordierite–sillimanite–quartz thermobarometers for spinel granulites in the central part of the Voronezh crystalline massif

Sample	Mineral assemblage and numbers of analyses in Tables 1–3	X_{Mg}		Thermobarometer				*P*, kbar	*Grt–Crd* thermometer					Average *T*, °C
				AP*		P(1)			T	HL	P(2)	E	B	
		Grt	*Cor*	*T*, °C	*P*, kbar	*T*, °C	*P*, kbar		temperature, °C					
3554/143a	*Grt*(8)–*Crd*(27)–*Sil*–*Qtz*–*Spl*	0.336	0.733	804	7.6	779	7.8	7.7	825	781	834	796	796	806
3554/143a	*Grt*(3)–*Crd*(6)–*Sil*–*Qtz*–*Spl*	0.335	0.751	767	7.3	743	7.3	7.3	783	746	795	758	770	770
3554/143a	*Grt*(6)–*Crd*(22)–*Sil*–*Qtz*–*Spl*	0.333	0.773	728	7.0	702	6.8	6.9	733	705	750	714	743	729
3554/143a	*Grt*(7)–*Crd*(3)–*Sil*–*Qtz*–*Spl*	0.333	0.761	751	7.2	722	7.0	7.1	759	726	772	736	759	750
3554/143a	*Grt*(2)–*Crd*(7)–*Sil-Qtz*–*Spl*	0.327	0.755	734	6.9	708	6.7	6.8	743	713	757	723	750	737
3554/143a	*Grt*(4)–*Crd*(25)–*Sil*–*Qtz*–*Spl*	0.325	0.780	701	6.7	675	6.4	6.5	703	680	721	687	725	703
3554/143a	*Grt*(9)–*Crd*(23)–*Sil*–*Qtz*–*Spl*	0.328	0.780	703	6.8	677	6.4	6.6	708	684	724	691	727	707
3554/143a	*Grt*(13)–*Crd*(24)–*Sil*–*Qtz*–*Spl*	0.311	0.796	654	6.3	626	5.7	6.0	649	634	669	638	695	657
3554/143a	*Grt*(1)–*Crd*(21)–*Sil*–*Qtz*–*Spl*	0.269	0.803	590	5.5	562	4.5	5.0	576	571	599	573	655	595
3554/143a	*Grt*(12)–*Crd*(26)–*Sil*–*Qtz*–*Spl*	0.285	0.784	617	5.7	590	4.9	5.3	631	619	652	624	685	642
3554/143b	*Grt*(72)–*Crd*(69)–*Sil*–*Qtz*–*Spl*	0.394	0.857	647	7.0	619	6.3	6.6	637	624	660	624	659	641
3550/6	*Grt*(5)–*Crd*(10)–*Sil*–*Qtz*–*Spl*	0.362	0.787	736	7.3	715	7.2	7.2	751	720	765	729	742	741
3550/6	*Grt*(2)–*Crd*(11)–*Sil*–*Qtz*–*Spl*	0.353	0.801	698	7.0	674	6.6	6.8	705	681	720	687	718	702
3550/6	*Grt*(4)–*Crd*(12)–*Sil*–*Qtz*–*Spl*	0.326	0.813	638	6.3	614	5.6	5.9	638	624	655	628	682	645

Note: Abbreviations for geothermobarometers and geothermometers: AP—Aranovich and Podlesskii (1989), P(1)—Perchuk *et al.* (1984); T—Thompson (1976), HL—Holdaway and Lee (1977); P(2)—Perchuk (1989), E—Ellis (1986), B—Bhattacharya *et al.* (1988).
* Calculated in accordance with the water-bearing model.

The maximum values are highly consistent with the stability field of the assemblage *Spl* + *Qtz*: $T > 800$°C at $P = 4$–8 kbar (Shulters and Bohlen, 1989; Waters, 1991, etc.). The magnetite exsolution textures in spinel also corroborate high temperatures during the metamorphism, because the magnetite–spinel solvus (Turnock and Eugster, 1962) suggests $T > 860$°C. The presence of ZnO and Fe^{3+} in the spinel expands the stability field of the *Spl* + *Qtz* assemblage to the lower temperature region, to 700–750°C (Shulters and Bohlen, 1989). This explains the occurrence of quartz and high-Zn spinel in physical contact in Sample 3550/9 (Fig. 3a).

The abundance of reaction textures with cordierite, spinel, sillimanite, and quartz made it possible to estimate the *P–T* metamorphic conditions by the spinel–cordierite thermometer (Vielzeuf, 1983) and the mutually consistent spinel–cordierite–quartz barometer and spinel–cordierite thermometer (Perchuk *et al.*, 1989; Gerya and Perchuk, 1990). The maximum values yielded by Vielzeuf's thermometer in application to the most ferrous cordierite and spinel are 756 and 815°C, they are in good agreement with the results of garnet–cordierite thermometry, and the temperature trend is generally compatible with that calculated based on garnet–cordierite equilibria. The *P–T* parameters can be estimated by the *Spl–Crd–Qtz* thermobarometer (Gerya and Perchuk, 1990) if the water activity is known, which, in turn, can be assayed by the *Grt–Bt–Kfs–Sil–Qtz* assemblage from Sample 3554/143a with the use of the procedure described by L.L. Perchuk in application to the calculation of *P–T* metamorphic paths and fluid conditions in the Sharyzhalgai Complex in the southeastern Baikal area (Perchuk, 1989). The values of a_{H_2O} are equal to 0.226–0.233 for pressures and temperatures close to the metamorphic culmination and 0.135–0.172 for the retrograde stage (Table 6). The *P–T* estimates based on spinel–cordierite thermometry and spinel–cordierite–quartz barometry are significantly lower than those yielded by the garnet–cordierite thermometer (Table 7). This seems to have been caused by the fact that the reactions participated by cordierite and spinel proceeded during the retrograde stage. This conclusion was also made by the authors of the spinel–cordierite–quartz thermobarometer during the study of spinel–cordierite granulites of the Kanskaya Formation in eastern Siberia (Perchuk *et al.*, 1989).

The *P–T* values obtained by garnet—cordierite–sillimanite–quartz themobarometry on three samples of the spinel-bearing granulites from the central part of the Voronezh crystalline massif define a generalized *P–T* path with the maximum values at 800–810°C and 7.6–7.8 kbar (Fig. 8, trend I). The minimum values, which reflect the closure of the garnet–cordierite system, are approximately 595°C and 5 kbar. The *P–T* path corresponds to a geothermal gradient of 1.3 kbar/100°C and is situated between the trends of isothermal decompression (ITD) and isobaric cooling (IBC). The *P–T* estimates yielded by spinel–cordierite–sillimanite thermobarometry define the lower temperature continuation of the path (Fig. 8, trend II), a fact that could be caused by exchange reactions between the cordierite and spinel and the development of late pyrite rims around the spinel during cordierite and spinel sulfidization.

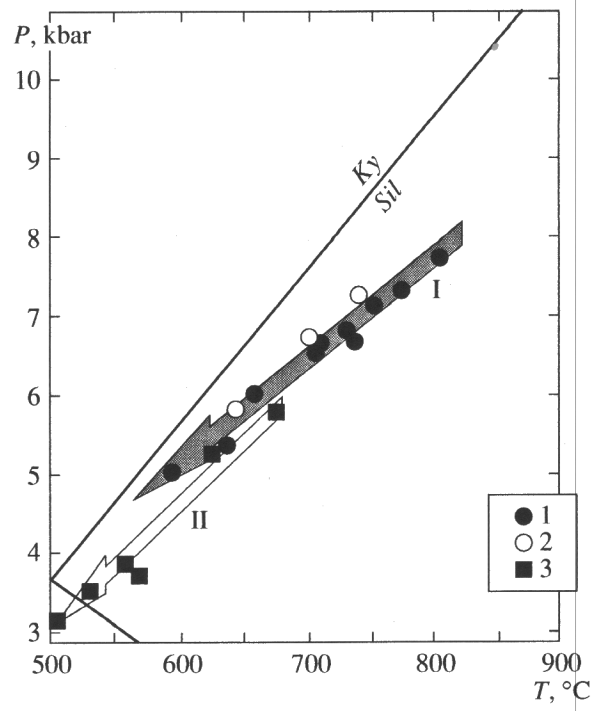

Fig. 8. Estimated *P–T* conditions and *P–T* path for spinel granulites from the Kursk–Besedino block.

Garnet–cordierite–sillimanite–quartz thermobarometry: (1) Sample 3554/143a; (2) Sample 3550/6; (3) spinel–cordierite–quartz thermobarometry.

P–T paths: (I) by garnet–cordierite–sillimanite–quartz thermobarometry; (II) by spinel–cordierite–quartz thermobarometry.

METAMORPHIC EVOLUTION OF GRANULITES IN THE CENTRAL PART OF THE KURSK MAGNETIC ANOMALY

The overwhelming majority of spinel–cordierite granulites retain evidence of their isobaric cooling after the metamorphic culmination. All of these granulite complexes were formed at moderate pressures and high temperatures under the effect of anomalous heat flux, which provides direct or indirect evidence of a magmatic source (Waters, 1991). Analyzing the relatively simple conceptual models for the geodynamic environments of metamorphism (England and Thompson, 1984; Sandiform and Powell, 1986; Harley, 1989; and others), one can conclude that "normal" collisional models (for example, those proposed by Ellis, 1987) are inapplicable to moderate-pressure granulites with traces of isobaric cooling. An anomalously high heat flux at moderate depths (20–30 km) could be brought about only by crustal extension and the ensuing ascent

Table 6. Water activity estimated by the assemblage *Grt–Bt–Kfs–Sil–Qtz*

Sample	Mineral assemblage and numbers of analyses in Tables 1–4	*P*, kbar	*T*, °C	a_{H_2O}
3554/143a	*Grt*(8)–*Bt*(28)–*Kfs*(17)–*Sil*–*Qtz*	7.7	804	0.233
3554/143a	*Grt*(12)–*Bt*(16)–*Kfs*(18)–*Sil*–*Qtz*	5.3	642	0.172

Table 7. *P–T* conditions of mineral equilibria estimated by the spinel–cordierite–quartz and spinel–cordierite thermobarometers for metapelitic granulites in the central part of the Voronezh crystalline massif

Sample	*Crd–Spl* pair	X_{Mg}^{Spl}	X_{Mg}^{Crd}	a_{H_2O}	Geothermometer		Geobarometer
					V	PGN	GP
					T, °C		*P*, kbar
3554/143a	*Spl*(5)–*Crd*(27)	0.272	0.733	0.233	815	673	5.9
3554/143a	*Spl*(6)–*Crd*(6)	0.272	0.751	0.233	756	623	5.2
3554/143a	*Spl*(3)–*Crd*(7)	0.246	0.755	0.172	673	555	3.9
3554/143a	*Spl*(2)–*Crd*(3)	0.244	0.761	0.172	650	532	3.5
3554/143a	*Spl*(8)–*Crd*(23)	0.245	0.780	0.172	601	502	3.1
3554/143a	*Spl*(10)–*Crd*(24)	0.233	0.796	0.172	538	429	1.9
3550/6	*Spl*(7)–*Crd*(10)	0.322	0.787	0.233	778	565	3.7
3550/6	*Spl*(8)–*Crd*(11)	0.303	0.801	0.172	679	480	2.2
3550/6	*Spl*(9)–*Crd*(12)	0.253	0.813	0.172	539	–	–
3504/381	*Spl*(4)–*Crd*(32)	0.222	0.781	0.172	548	403	1.2
3504/381	*Spl*(5)–*Crd*(34)	0.219	0.772	0.172	561	418	1.4

Note: Geothermobarometry: V—Vielzeuf (1983), PGN—Perchuk *et al.* (1989), GP—Gerya and Perchuk (1990).

of the asthenospheric layer to higher levels or by magmatic "accretion" at the basement of the crust (Wells, 1980; Bohlen, 1991). The later mechanism has fairly strong limitations in terms of the volume of magmatic material present in the crust (Waters, 1991); hence, the most feasible explanation seems to be the extension of the crust, which has been previously thickened by collision, and its reduction to the "normal" thickness.

Earlier, I have obtained data on the evolution of mafic granulites in the Kursk–Besedino part of the Voronezh crystalline massif. The rocks provide evidence of two independent metamorphic events in the Early Archean and Late Proterozoic. The Early Archean metamorphic stage is characterized by a subisobaric cooling path over the intervals of 784–684°C and 5.6–4.2 kbar (Savko, 1999). The Early Proterozoic stage was related to active tectonism and collision, which resulted in crustal thickening and the descent of the granulites to depths of 25–30 km. The Early Proterozoic metamorphism affected not only the Archean granulites but also the overlying younger Precambrian rocks. Consequently, the mineral assemblages of the granulites were readjusted to the pressures of 6.8–8.7 kbar and temperatures of 665–771°C.

The close spatial association of metapelitic and mafic granulites suggests that they suffered the same metamorphic and tectonic transformations. The mineral assemblages of the metapelitic granulites do not preserve evidence of the Early Archean metamorphic event, which occurred at high temperatures (of approximately 800°C) and relatively low pressures (4.2–5.6 kbar). The spinel-bearing granulites append the information obtained on subisobaric cooling during the Early Proterozoic metamorphic episode. The maximum *P–T* values obtained for mineral assemblages in the metapelitic and mafic granulites are very close. Unfortunately, the latter rocks provide no evidence on the retrograde evolution after the metamorphic culmination during the Early Proterozoic metamorphic event. Hence, the mineral assemblages of the cordierite–spinel granulites make it possible to elucidate the latest Precambrian metamorphic evolution of the central Voronezh crystalline massif. The evolutionary scenario can be briefly summarized as follows:

(1) Early Archean. The stage was characterized by high-temperature, moderate-pressure metamorphism and subsequent isobaric cooling. The Early Archean granulite metamorphism was caused by the tectonic thickening of the Archean crust as a consequence of collision (?). The nearly isobaric cooling of the rocks was brought about by the cooling of syntectonic plutons (Savko, 1999).

(2) From the Late Archean throughout the Early Proterozoic, the central portion of the Kursk Magnetic

Anomaly area was characterized by the deposition (on an Early Archean basement) of a thick Late Archean volcanogenic Mikhailovskaya Formation and a series of Early Proterozoic volcanic–terrigenous and jaspilite sequences (with a total thickness of 10–15 km).

(3) Early Proterozoic. At 2000 ± 100 Ma, active tectonism and collision folded the Late Archean and Early Proterozoic rocks, which were intruded by numerous magmatic bodies. The Early Proterozoic sediments overlaying the granulites were metamorphosed to the upper greenschist–upper amphibolite facies (4–6 kbar and 450–700°C; Savko, 1994a, 1994b; Gerasimov and Savko, 1995). The granulites were brought to depths of approximately 30 km by tectonic crustal thickening, and their mineral assemblages were affected by Early Proterozoic metamorphism. The rocks were cooled at decreasing pressure during the extension of the crust and the reduction of its thickness to the normal level.

CONCLUSION

This paper presents the results of a petrologic study of cordierite–spinel granulites in the central part of the Kursk Magnetic Anomaly megablock in the Voronezh crystalline massif. The rocks bear diverse reaction textures with spinel, cordierite, sillimanite, magnetite, and pyrite. In addition to reaction textures commonly detected in rocks of this type (cordierite rims around spinel, spinel and quartz inclusions in garnet), the granulites contain rims of pyrite with sillimanite around Zn-rich spinel and sillimanite–cordierite rims around sulfides, which provide evidence of the sulfidization of the cordierite and spinel due to a significant increase in the sulfur activity late during the retrograde metamorphic stage.

The *P–T* trend obtained with the help of garnet–cordierite–sillimanite–quartz thermobarometry reflects the subisobaric cooling of the granulites from 800–810°C and 7.6–7.8 kbar to 595°C and 5 kbar. The metamorphic evolution of the spinel granulites was caused by the extension of the crust (which had been thickened during Early Proterozoic collision) and its reduction to the normal thickness.

ACKNOWLEDGMENTS

Several issues of this paper were discussed with S.P. Korikovsky and V.Yu. Gerasimov (Institute of the Geology of Ore Deposits, Petrography, Mineralogy, and Geochemistry, Russian Academy of Sciences), and this helped the author to improve the text of the manuscript. The author took into account valuable comments made by T.V. Gerya (Institute of Experimental Mineralogy, Russian Academy of Sciences) during the reviewing of the paper. N.N. Kononkova (Vernadsky Institute of Geochemistry and Analytical Chemistry, Russian Academy of Sciences) and N.N. Korotaeva (Moscow State University) helped in the analytical work. The author thanks all aforementioned persons.

This study was financially supported by the Russian Ministry of General and Special Education and the Moscow State Geological Prospecting Academy (Project NICh-823).

REFERENCES

Aranovich, L.Ya. and Podlesskii, K.K., Geothermobarometry of High-Grade Metapelites: Simultaneously Operating Reactions, Daly, J.S., Cliff, R.A., Yardley, B.W.D., Eds., in *Evolution of Metamorphic Belts. Geol. Soc. Spec. Publ.*, London: 1989, no. 43, pp. 45–61.

Artemenko, G.V., *Geokhronologicheskaya korrelyatsiya vulkanizma i granitoidnogo magmatizma yugo-vostochnoi chasti Ukrainskogo shchita i Kurskoi magnitnoi anomalii* (Geochronological Correlation between Volcanism and Granitoid Magmatism in the Southeastern Part of the Ukrainian Shield and the Kursk Magnetic Anomaly), Kiev: Naukova Dumka. Geokhimiya i Rudoobrazovanie, 1995, no. 21, pp. 129–154.

Bhattacharya, A., Mazumdar, A.C., and Sen, S.K. Fe–Mg Mixing in Cordierite: Constraints from Natural Data and Implications for Cordierite–Garnet Geothermometry in Granulites, *Am. Mineral.*, 1988, vol. 73, no. 3/4, pp. 338–344.

Bohlen, S.R., On the Formation of Granulites, *J. Metamorph. Geol.*, 1991, vol. 9, pp. 223–229.

Clarke, G.L. and Powell, R., Decompressional Coronas and Symplectites in Granulites of the Musgrave Complex, Central Australia, *J. Metamorph. Geol.*, 1991, vol. 9, pp. 441–450.

Clarke, G.L., Powell, R., and Guiraud, M., Low-Pressure Granulite Facies Metapelitic Assemblages and Corona Textures from McRobertson Land, East Antarctica: The Importance of Fe_2O_3 and TiO_2 in Accounting for Spinel-bearing Assemblages, *J. Metamorph. Geol.*, 1989, vol. 7, pp. 323–335.

Dasgupta, S., Sengupta, P., Ehl, J., Raith, M., and Bardham, S., Reaction Structures in a Suite of Spinel Granulites from the Eastern Ghats Belt, India: Evidence for Polymetamorphism, a Partial Petrogenetic Grid in the System KFMASH and the Roles of ZnO and Fe_2O_3, *J. Petrol.*, 1995, vol. 36, no. 2, pp. 435–461.

Ellis, D.J., Garnet–Liquid Fe^{2+}–Mg Equilibria and Implication for the Beginning of Melting in the Crust and Subduction Zones, *Am. J. Sci.*, 1986, vol. 286, pp. 765–791.

Ellis, D.J., Origin and Evolution of Granulites in Normal and Thickened Crusts, *Geology*, 1987, vol. 15, pp. 167–170.

England, P.C. and Thompson, A.B., Pressure–Temperature–Time Paths of Regional Metamorphism: I. Heat Transfer during the Evolution of Regions of Thickened Continental Crust, *J. Petrol.*, 1984, vol. 25, part 4, pp. 894–928.

Fonarev, V.I., Graphchikov, A.A., and Konilov, A.N., A Consistent System of Geothermometers for Metamorphic Complexes, *Int. Geol. Rev.*, 1991, vol. 33, no. 8, pp. 743–783.

Gerasimov, V.Yu. and Savko, K.A., Geospeedometry and Temperature Evolution of Garnet–Cordierite Metapelites in the Voronezh Crystalline Massif, *Petrologiya*, 1995, vol. 3, no. 6, pp. 563–577.

Gerya, T.V. and Perchuk, L.L., GEOPATH: a New Computer Program for Geothermobarometry and Related Calculations with the IBM PC Computer, *15th General Meeting Int. Mineral. Assoc., Beijing*, Abstracts, 1992, vol. 2, p. 1010.

Gerya, T.V. and Perchuk, L.L., Evolution of the Thermodynamic Conditions in Granulites of the Angara–Kansk Uplift, *Vestn. Mosk. Univ., Geol.*, 1990, no. 6, pp. 35–49.

Guidotti, C.V., Transition from Staurolite to Sillimanite Zone, Rangeley Quadrangle, *Bull. Geol. Soc. Am.*, 1974, vol. 85, pp. 475–490.

Harley, S.L., The Origin of Granulites: a Metamorphic Perspective, *Geol. Magazine*, 1989, vol. 126, no. 3, pp. 215–247.

Holdaway, M.J. and Lee, S.M. Fe–Mg Cordierite Stability in High-Grade Pelitic Rocks Based on Experimental, Theoretical, and Natural Observations, *Contrib. Mineral. Petrol.*, 1977, vol. 63, pp. 175–198.

Korikovsky, S.P., *Fatsii metamorfizma metapelitov* (Metamorphic Facies of Metapelites), Moscow: Nauka, 1979.

Perchuk, L.L., *P–T*–Fluid Regimes of Metamorphism and Related Magmatism with Specific Reference to the Granulite-Facies Sharyzhalgay Complex of Lake Baikal, *Evolution of Metamorphic Belts. Geol. Soc. Spec. Publ.*, Daly, J.S., Cliff, R.A, Yardley, B.W.D, Eds., London: 1989, no. 42, pp. 275–291.

Perchuk, L.L., Gerya, T.V., and Nozhkin, A.D., Petrology and Retrograde *P–T* Path in Granulites of the Kanskaya Formation, Yenisey Range, Eastern Siberia, *J. Metamorph. Geol.*, 1989, vol. 7, pp. 599–617.

Perchuk, L.L., Lavrent'eva, I.V., Kotelnikov, A.R., and Petrik, I., Comparative Characteristics of Metamorphism Thermodynamic Regimes for Rocks of the Major Caucasian Range and Western Carpathians, *Geol. Zborn.—Geol. Carpathica*, 1984, vol. 35, no. 1, pp. 105–155.

Perchuk, L.L., Consistence of Some Fe–Mg Geothermometers Based on the Nernst Law, *Geokhimiya*, 1989, no. 5, pp. 611–622.

Sandiford, M. and Powell, R., Deep Crystal Metamorphism during Continental Extension: Modern and Ancient Examples, *Earth Planet. Sci. Lett.*, 1986, vol. 79, pp. 151–158.

Savko, K.A., *Granulity Voronezhskogo kristallicheskogo massiva, petrologiya i evolyutsiya metamorfizma* (Granulites of the Voronezh Crystalline Massif: Petrology and the Evolution of Metamorphism), Voronezh: Voronezh. Gos. Univ., 1999.

Savko, K.A., Fayalite–Grunerite–Magnetite–Quartz Rocks of the Fe-rich Association in the Voronezh Crystalline Massif, *Petrologiya*, 1994a, vol. 2, no. 5, pp. 540–550.

Savko, K.A., Sillimanite–Muscovite Zone in the Metamorphic Complex of the Vorontsov Group, Voronezh Crystalline Massif, *Geol. Geofiz.*, 1994b, no. 6, pp. 73–86.

Savko, K.A., Zinc Staurolite in High-Grade Gneisses of the Voronezh Crystalline Massif, *Vestn. Voronezh. Univ. Ser. Geol.*, 1997, no. 3, pp. 76–84.

Sengupta, P., Karmakar, S., Dasgupta, S., and Fukuoka, M., Petrology of Spinel Granulites from Araku, Eastern Ghats, India, and a Petrogenetic Grid for Sapphirine-free Rocks in the System FMAS, *J. Metamorph. Geol.*, 1991, vol. 9, pp. 451–459.

Shulters, J.C. and Bohlen, S.R., The Stability of Herzinite and Herzinite–Gahnite Spinels in Corundum- or Quartz-bearing Assemblages, *J. Petrol.*, 1989, vol. 30, part 4, pp. 1017–1031.

Thompson, A.B., Mineral Reactions in Pelitic Rocks. II. Calculations of Some *P–T–X*(Fe–Mg) Phase Relations, *Am. J. Sci.*, 1976, vol. 276, pp. 425–454.

Turnock, A.V. and Eugster, M.P. Fe–Al Oxides: Phase Relationships below 1000°C, *J. Petrol.*, 1962, vol. 3, pp. 533–565.

Vielzeuf, D., The Spinel and Quartz Associations in High Grade Xenoliths from Tallante (S.E. Spain) and Their Potential Use in Geothermometry and Barometry, *Contrib. Mineral. Petrol.*, 1983, vol. 82, pp. 301–311.

Warren, R.G. and Stewart, A.J., Isobaric Cooling of Proterozoic High-Temperature Metamorphites in the Northern Arunta Block, Central Australia: Implications for Tectonic Evolution, *Precambrian Res.*, 1988, vol. 40/41, pp. 175–198.

Waters, D.J., Herzinite–Quartz Granulites: Phase Relations and Implications for Crustal Processes, *Eur. J. Mineral.*, 1991, vol. 3, pp. 367–386.

Wells, P.R.A., Thermal Models for the Magmatic Accretion and Subsequent Metamorphism of Continental Crust, *Earth Planet. Sci. Lett.*, 1980, vol. 46, pp. 253–265.